Cell Metabolism

Resource

Deciphering the decline of metabolic elasticity in aging and obesity

Graphical abstract

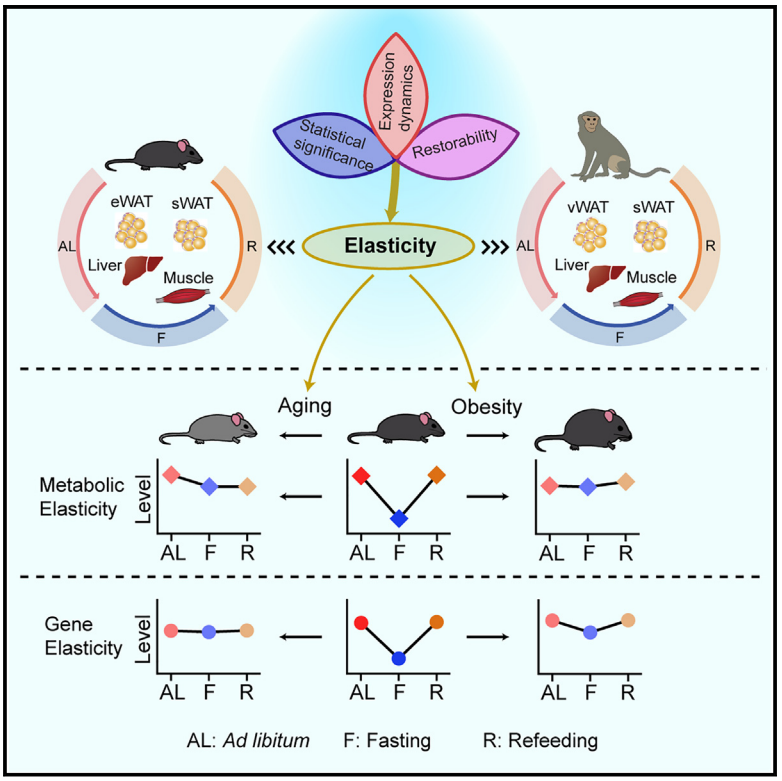

Highlights

- Elasticity scores are developed to quantify the ability to restore homeostasis
- Elasticity is profiled across metabolically active tissues in mice and monkeys
- Metabolic and gene elasticity decline during aging and with obesity

Authors

Qiuzhong Zhou, Lexiang Yu, Joshua R. Cook, Li Qiang, Lei Sun

Correspondence

lq2123@cumc.columbia.edu (L.Q.), sun.lei@duke-nus.edu.sg (L.S.)

In brief

We designed a "metabolic elasticity" scoring system measuring an organism's capacity to cope with and recover from metabolic fluctuations. With age and obesity, this elasticity notably diminishes, shedding light on the fundamental causes of metabolic degradation in these conditions.

Zhou et al., 2023, Cell Metabolism *35*, 1661–1671
September 5, 2023
https://doi.org/10.1016/j.cmet.2023.08.001

CellPress

Cell Metabolism

CellPress

Resource

Deciphering the decline of metabolic elasticity in aging and obesity

Qiuzhong Zhou,[1,4] Lexiang Yu,[2,3,4] Joshua R. Cook,[3] Li Qiang,[2,3,*] and Lei Sun[1,5,*]
[1]Cardiovascular and Metabolic Disorders Program, Duke-NUS Medical School, Singapore, Singapore
[2]Naomi Berrie Diabetes Center and Department of Pathology and Cell Biology, Columbia University, New York, NY, USA
[3]Department of Medicine, Columbia University, New York, NY, USA
[4]These authors contributed equally
[5]Lead contact
*Correspondence: lq2123@cumc.columbia.edu (L.Q.), sun.lei@duke-nus.edu.sg (L.S.)
https://doi.org/10.1016/j.cmet.2023.08.001

SUMMARY

Organisms must adapt to fluctuating nutrient availability to maintain energy homeostasis. Here, we term the capacity for such adaptation and restoration "metabolic elasticity" and model it through *ad libitum*-fasting-refeeding cycles. Metabolic elasticity is achieved by coordinate versatility in gene expression, which we call "gene elasticity." We have developed the gene elasticity score as a systematic method to quantify the elasticity of the transcriptome across metabolically active tissues in mice and non-human primates. Genes involved in lipid and carbohydrate metabolism show high gene elasticity, and their elasticity declines with age, particularly with PPARγ dysregulation in adipose tissue. Synchronizing PPARγ activity with nutrient conditions through feeding-timed agonism optimizes their metabolic benefits and safety. We further broaden the conceptual scope of metabolic and gene elasticity to dietary challenges, revealing declines in diet-induced obesity similar to those in aging. Altogether, our findings provide a dynamic perspective on the dysmetabolic consequences of aging and obesity.

INTRODUCTION

Aging is a complex biological process characterized by long-term deterioration of bodily functions. The multifactorial nature of the aging process—including contributions from genetics, environment, diet, and lifestyle—crystallizes within a gradually evolving, ultimately maladaptive metabolic response to nutrient environments. The importance of such age-related disruption of nutrient sensing to health and longevity is reflected in the impact of genetically or pharmacologically manipulating key nutrient-sensing pathways, including those downstream of insulin/insulin growth factor (IGF), mTOR, AMPK, and sirtuins.[1–3] A hallmark of aging is declining metabolic flexibility, which refers to the inefficient switch of fuel utilization between carbohydrates and fatty acids according to their relative availability.[4–6] Although metabolic flexibility nicely describes discrete biochemical adjustments that occur during the transition between feeding states, it does not speak to the broader battery of physiologic changes that defend metabolic homeostasis against the challenges of daily life.

In a modern society, nutrient scarcity is usually transient and often quickly reverts to nutrient abundance, requiring the body to adapt its metabolic program accordingly. The ability to efficiently redirect and then restore metabolic processes in response to temporary stresses is not accurately described by existing terminology such as metabolic flexibility. Here, we introduce "metabolic elasticity" to signify the ability of an organism to respond to a disturbance in energy balance and return to its baseline metabolic homeostasis. Metabolic elasticity likely relies upon underlying elasticity in the expression of metabolically relevant genes. In order to characterize this relationship, we developed a scoring system that integrates gene-expression dynamics, restorability, and statistical significance in key metabolic organs during an *ad libitum*-fasting-refeeding (AL-F-R) cycle. Using this rubric, we discovered aging-associated declines in both metabolic and gene-expression elasticity. Importantly, we identified PPARγ as the top transcriptional regulator of elastic genes in adipose tissue. Manipulating gene-expression elasticity by reinforcing PPARγ activity results in a feeding status-dependent improvement in metabolic health. To broaden the metabolic elasticity concept, we examined the metabolic elasticity and gene elasticity score (GElaS) in diet-induced obesity and found similar impairments in metabolic and gene-expression elasticity as in aging. In sum, our study introduces metabolic elasticity as an effective means of assessing metabolic health and a feasible strategy to curb metabolic decline in aging and obesity.

RESULTS

Developing a gene-expression elasticity score system to quantify metabolic elasticity

Organisms often enter an energy-conserving adaptive state upon caloric deprivation and revert to the previously established

homeostatic state after resolution of the disturbance, requiring the body to expediently redirect metabolic processes to tightly maintain energy balance. We adopt the term "metabolic elasticity" to describe the efficiency of such adaptation. We see metabolic elasticity play out, for example, in the reduction and subsequent restoration of the metabolic parameters such as circulating levels of glucose, insulin, and free fatty acids (FFAs) across an AL-F-R cycle in mice (Figure 1A). Such elasticity also manifests in other metabolic parameters such as body weight, including both lean and fat components (Figure 1A).

Maintaining metabolic elasticity should largely rely upon elastic alterations at the transcriptome level, which we refer to as "gene elasticity." To establish gene elasticity, we performed RNA sequencing (RNA-seq) for four major metabolic organs, including epididymal white adipose tissue (eWAT), subcutaneous WAT (sWAT), liver, and muscle, during an AL-F-R cycle in healthy young mice (Figure 1B). As expected, the *ad libitum* and refeeding samples are largely grouped together while fasting samples remain distinct in the principal-component analysis (PCA), indicating that the transcriptome is elastic and can revert to the pre-established baseline state after refeeding (Figure S1A). "Expression dynamics" is often used to describe alterations in the transcriptome or gene expression between two metabolic states. However, this term does not include the restoration of the transcriptome to its original state following the resolution of a nutrient challenge. We thus introduced an additional analytic factor to expression dynamics—restorability—which represents the extent to which genes can bounce back to their *ad libitum* expression after an AL-F-R cycle (Figure 1C). In order to concisely quantify this analysis, we developed the GElaS, which integrates expression dynamics, restorability, and statistical significance into a single metric of metabolic elasticity at the gene level (Figure 1C) (detailed in STAR Methods).

GElaS correlates strongly with dynamic changes in gene expression (i.e., fold changes between F and AL or R and F) during the AL-F-R cycle. Genes with low GElaS change little in their expression during fasting or refeeding, while those with high GElaS exhibit stronger changes in expression (Figures 1D and S1B). We must emphasize that GElaS is not equivalent to expression dynamics. Each tissue we examined expresses some genes with low GElaS despite high expression dynamics during a nutrient challenge (Figures 1E and S1C). This is because the integrative design of GElaS also heavily weighs genes' statistical significance and restorability during an AL-F-R cycle (Figure S1D).

Elastic genes are enriched in lipid and carbohydrate metabolism

To examine the functional relevance of GElaS, we ranked genes according to their GElaS and conducted gene ontology (GO) analysis in a sliding window of 500-gene width across the rank. Genes with high GElaS are connected to a large number of GO terms, while genes with low GElaS are much less related to biological pathways (Figures 1F and S1E). The GOs associated with top GElaS genes are enriched in lipid and carbohydrate metabolism (Figure 1G), congruent with the prominence of lipid- and carbohydrate-metabolic genes among the highest GElaS: *Angptl8*, *Irf4*, *Dgat2*, *Pnpla3*, *Scd2*, *Lep*, *Acyl*, and *Pdk4* in the eWAT and *Angptl8*, *Gck*, *Igfbp1*, *Pcsk9*, *Cidec*, *Fgf21*, and *Fasn* in the liver (Figure 1H). Furthermore, the top 500 GElaS genes in distinct metabolic organs demonstrate significant overlap, with the highest degree of overlap observed between eWAT and iWAT (Figures S1F and S1G), suggesting that the regulatory mechanisms underlying GElaS tend to be conserved across different organs.

Cell-type heterogeneity within each tissue[7–9] calls into question the specific source(s) of metabolic elasticity. We employed several single-nucleus/-cell RNA-seq datasets to assess the distribution of elastic genes in different cell populations within each organ. In adipose tissue, the genes with top GElaS are preferentially expressed in adipocytes, while the genes with low GElaS are broadly detected in all cell types (Figures 1I and S1H). Similarly, the most elastic genes in liver are preferentially distributed in hepatocytes (Figure S1I). Collectively, these data suggest that metabolic elasticity arises mainly from the defining metabolic cell type of each organ.

The enrichment of elastic genes in lipid and carbohydrate metabolism is recapitulated in non-human primates

The relevance of metabolic elasticity extends beyond mice to non-human primates, as we observed during an AL-F-R cycle in crab-eating macaques (Figure 2A). To test if the GElaS system is applicable to higher mammals, we conducted RNA-seq followed by GElaS analysis on biopsies of subcutaneous and visceral (omental) WATs (sWAT and vWAT), liver, and muscle from 12 adult crab-eating macaques (9.4–20.3 years old) during *ad libitum*, fasting, and refed states (Figure 2B). Similar to our observations in mice, genes with high GElaS show stronger expression changes during the AL-F-R cycle than genes with low GElaS (Figures 2C and S2A). High-GElaS genes are also more connected than low-GElaS genes to GO terms (Figures 2D and S2B), particularly lipid and carbohydrate metabolism pathways (Figures 2E and S2C). Indeed, key players in energy metabolism feature prominently among the topmost elastic genes. These include as *PCK1*, *APOLD1*, and *SREBF1* in vWAT; *SREBF1*, *PCK1*, and *PNPLA3* in sWAT; *GCK*, *FGF21*, and *SREBF1* in liver; and *DDIT4*, *SREBF1*, and *MYOD1* in muscle (Figures 2F and S2D). To determine if the GElaS correlates across species, we plotted the elastic genes with GElaS > 0.5 in each species and found a clear positive association (Figures 2G and S2E). Key metabolic regulators, including *SREBF1*, *PCK1*, and *ANGPTL4*, number among the top elastic genes in both species (Figure 2G). The poor correlation in sWAT may be due to distinct subcutaneous depots harvested from mice (inguinal) and monkeys (abdominal). Also as in mice, overlaying single-nucleus gene-expression data[10] on GElaS reveals that gene elasticity tends to be confined to the major metabolic cell type of each tissue (i.e., adipocytes in WAT; hepatocytes in liver), while those with low GElaS do not show cell-type specificity within tissues (Figures 2H and 2I).

Metabolic elasticity and GElaS decline during aging

Although we have focused on nutrient conditions per se as drivers of metabolic and gene elasticity, these effects depend heavily on age. Aging blunts metabolic elasticity, significantly attenuating the dynamism of multiple metabolic parameters across the AL-F-R cycle, including fat and lean mass, blood glucose, and FFA levels (Figures 3A and S3A). These age-related

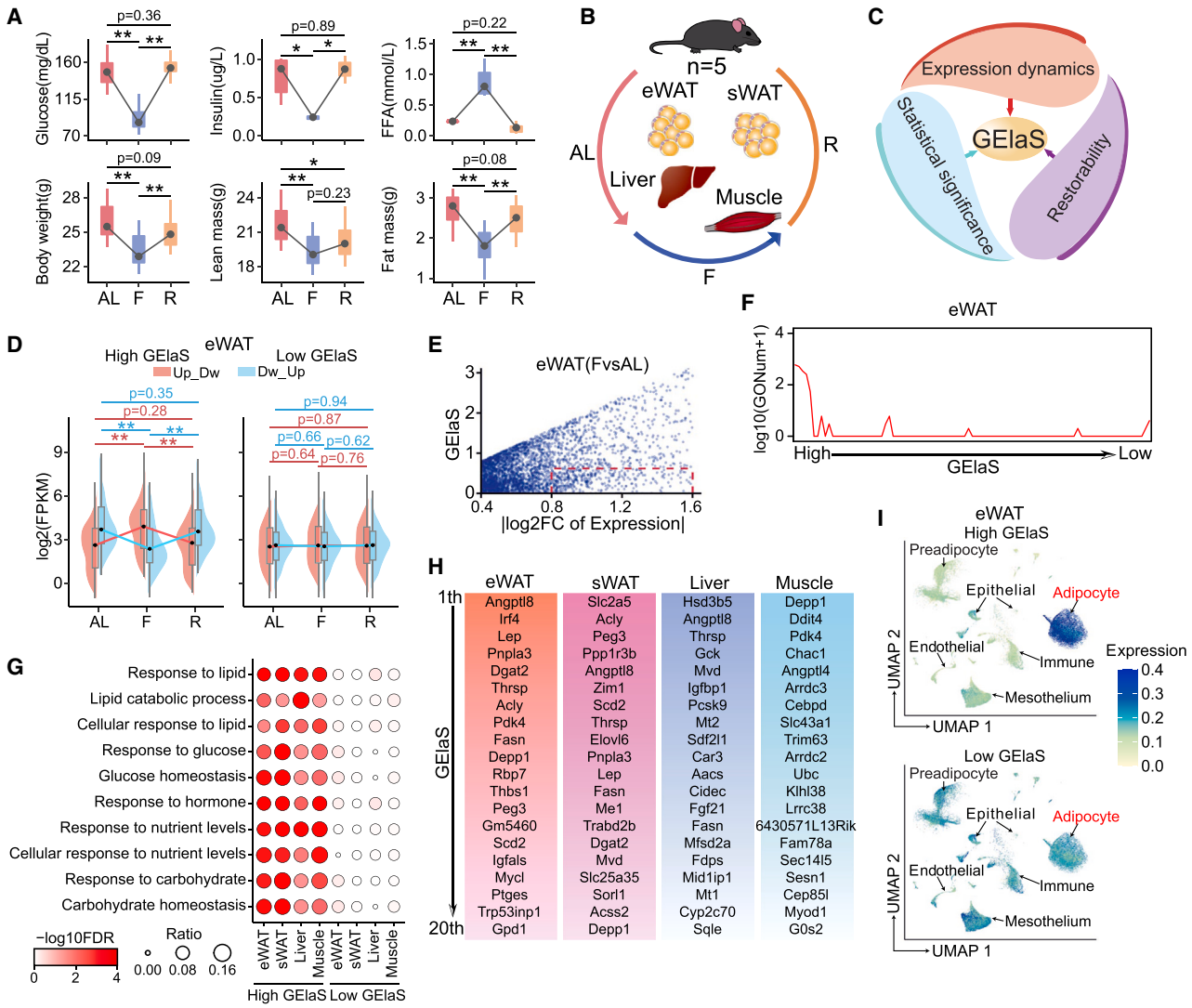

Figure 1. Gene elasticity is connected to major metabolism pathways

(A) Elastic changes of metabolic parameters including glucose, insulin, FFA, body weight, lean mass, and fat mass. The dots indicate the median values. The boxes cover the range from 25% (Q1) to 75% (Q3) quantile (*p < 0.05, **p < 0.01, one-way ANOVA with Tukey's test).

(B) A schematic diagram of RNA-seq samples of metabolic organs harvested at different nutrient states.

(C) Gene elasticity score (GElaS) is integrated from expression dynamics, restoration extent, and statistical significance during an AL-F-R cycle. AL, *ad libitum*; F, fasting; R, refeeding.

(D) Dynamic changes of the high (top 500) and low (bottom 500) GElaS genes in eWAT during an AL-F-R cycle. Each group of genes is further divided into fasting_up-refeeding_down (Up_Dw) and fasting_down-refeeding-up (Dw_Up) regulated subgroups. The distribution of gene expression (log_2fragments per kilobase per million [FPKM]) for each subgroup is plotted across AL, F, and R states. The violin plot indicates the distribution of gene expression. The dot is the median value of gene expression. The box covers an expression range from 25% (Q1) to 75% (Q3) quantile (*p < 0.05, **p < 0.01, Mann-Whitney test).

(E) The relationship between dynamic changes (log_2foldchange [FC] of expression) upon fasting (FvsAL) and GElaS in eWAT.

(F) The numbers of enriched GO (biological processes category) in a 500-gene window sliding across the GElaS rank in eWAT. The window slides with a 100-gene step length from high to low GElaS.

(G) GOs enriched in genes with high (top 500) and low (bottom 500) GElaS are plotted across each examined metabolic organ. The criterion of enrichment is false discovery rate (FDR) < 0.1. The lipid and carbohydrate biological pathways are enriched in high-GElaS but not low-GElaS genes.

(H) Top 20 elastic genes in each metabolic organ.

(I) The gene-expression distribution of genes with high (top 500) and low GElaS (bottom 500) across different cell populations in eWAT. The color indicates the average expression of the high- or low-elastic genes in each cell type in the visualization of uniform manifold approximation and projection (UMAP).

impairments in metabolic elasticity are likely driven by concordant reductions in gene elasticity. Consistent with this possibility, lipid- and carbohydrate-metabolic pathways that are down-regulated during aging[11,12] are particularly enriched in highly elastic genes (Figure 3B), supporting an interaction between GElaS and the aging process.

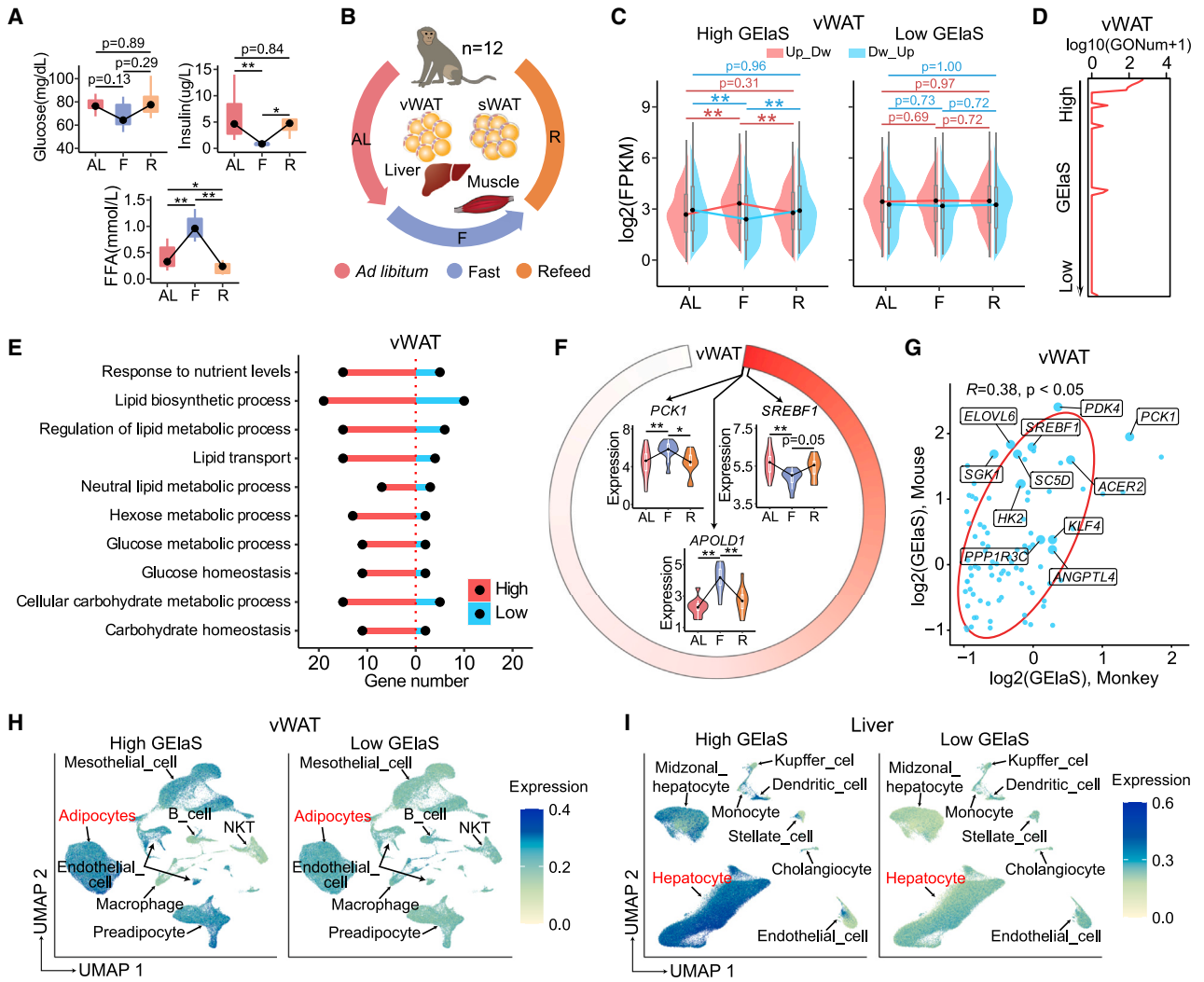

Figure 2. Gene elasticity in the non-human primate crab-eating macaques

(A) Elastic changes of metabolic parameters including glucose, insulin, and FFA during the AL-F-R cycle in crab-eating macaques. The dots indicate the median values. The boxes cover the range from 25% (Q1) to 75% (Q3) quantile (*p < 0.05, **p < 0.01, one-way ANOVA with Tukey's test).

(B) A schematic diagram for RNA-seq samples in the metabolic organs from the non-human primate crab-eating macaques.

(C) Dynamic changes in an AL-F-R cycle between the high (top 500) and low (bottom 500) GElaS genes in vWAT of crab-eating macaques. Up_Dw and Dw_Up indicate the fasting_up-refeeding_down and fasting_down-refeeding-up regulated subgroups, respectively. The distribution of gene expression (log_2FPKM) for each subgroup is plotted across AL, F, and R states. The violin plot indicates the distribution of gene expression. The dot is the median value of gene expression. The box covers an expression range from 25% (Q1) to 75% (Q3) quantile (*p < 0.05, **p < 0.01, Mann-Whitney test).

(D) The numbers of enriched GO (biological processes category) in a 500-gene window sliding from the high to low GElaS in vWAT. The step length is 100 bp for slide-window analysis.

(E) Number of the gene in association with the lipid, glucose, and carbohydrate metabolism in the high (top 500) and low (bottom 500) GElaS genes in vWAT.

(F) Several key metabolic regulators such as *PCK1*, *APOLD1*, and *SREBF1* are in the top of GElaS rank in vWAT. Circle color indicates the GElaS rank. y axis represents the expression (log_2FPKM). p value was calculated by limma and adjusted by Benjamini and Hochberg method (*FDR < 0.05, **FDR < 0.01).

(G) Scatterplot for elastic genes (GElaS > 0.5) in monkey and mouse. x axis is the log_2(GElaS) for monkey, while y axis represents the log_2(GElaS) for mouse. The correlation analysis was performed by Pearson's correlation.

(H and I) The gene-expression distribution of genes with high (top 500) and low GElaS (bottom 500) across different cell populations in vWAT and liver, separately. The color indicates the average expression of the high- or low-elastic genes in each cell type in the UMAP visualization.

To examine the implications of gene elasticity for aging, we calculated the number of aging-regulated genes (AR genes)[11] within a 500-gene window sliding across GElaS rank. Across all examined organs in both mouse and human, gene windows at the high-GElaS end contain a larger number of AR genes (Figures S3B and S3C). Further, genes with high GElaS exhibit age-related changes in expression that are greater in both magnitude (Figures S3D and S3E) and dynamism (i.e., larger standard deviations over time) (Figure S3F) than those genes with low GElaS. In an expression-independent analysis, we

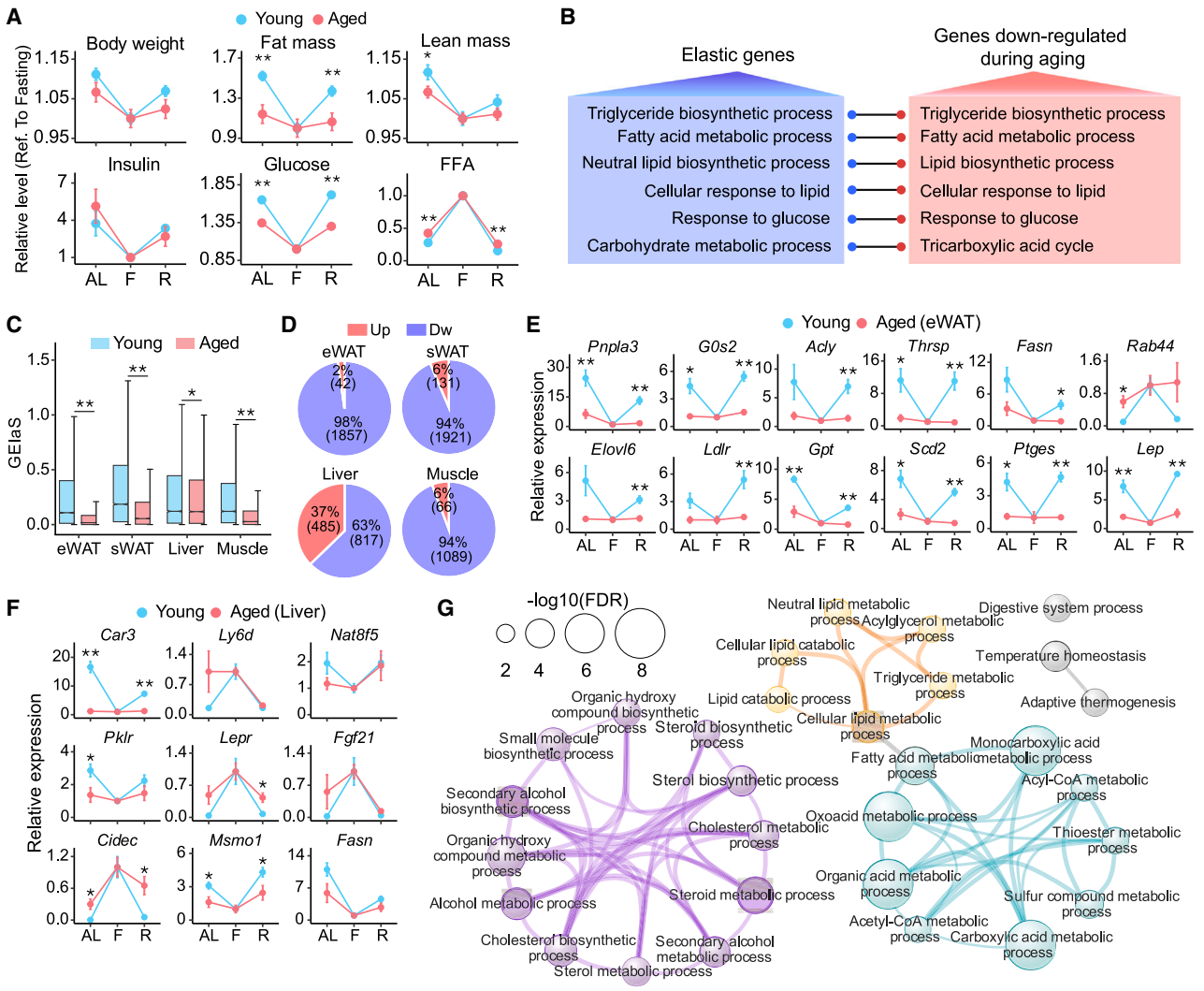

Figure 3. Gene elasticity is impaired during aging

(A) The relative values of body weight, fat mass, lean mass, insulin, glucose, and FFA in one AL-F-R cycle. The values are normalized to the fasting state of young and aged mice, respectively.

(B) The biological pathways in association with the elastic genes (blue) and the genes downregulated during aging (red).

(C) The GElaS distribution in young and aged samples. The box covers a GElaS range from 25% (Q1) to 75% (Q3) quantile. The black line in the box represents the median value of GElaS. The statistical significance of GElaS average was conducted by Mann-Whitney test.

(D) The number of differential elastic genes between the young and aged mice. Up, upregulated genes; Dw, downregulated genes.

(E) Relative expression determined by real-time PCR for the differential elastic genes in eWAT. The gene expression is normalized to and scaled by the expression of fasting state in both young and aged samples.

(F) Relative expression by real-time PCR for the differential elastic genes in liver.

(G) Functional enrichment (top 30) for the differential elastic genes with decreased GElaS during aging (eWAT).

Data are represented as mean ± SEM (A, E, and F). *p < 0.05, **p < 0.01, two-sided Student's t test (A, E, and F) or Mann-Whitney test (C).

employed genome-wide association study (GWAS) datasets (GWAS Catalog of EBI, gwas_catalog_v1.0.2)[13] and calculated the number of genes bearing aging trait-associated SNPs in elastic versus non-elastic genes. Across both WAT depots and liver, we found a higher proportion of genes connected to aging traits in the elastic group (Figure S3G), supporting the relevance of gene elasticity to human genetics in the context of aging.

These results indicate that aging preferentially affects the abundance of elastic genes (Figures S3D–S3F). However, it is unknown if aging affects gene elasticity per se, as genes' elasticity depends on their response to nutrient fluctuations rather than their transcript abundance. To directly assess the impact of aging on gene elasticity, we performed RNA-seq on metabolic organs in 18-month-old mice during an AL-F-R cycle. In keeping with the age-related loss of metabolic elasticity, GElaS declines with age across all examined organs (Figure 3C). This concerted loss of both metabolic and gene elasticity may explain the widely appreciated decline in metabolic health during aging.[5,14,15]

To identify genes whose elasticity is most affected by aging, we set $|GElaS_{aged} - GElaS_{Young}| = |\Delta GElaS| > 0.5$ as the

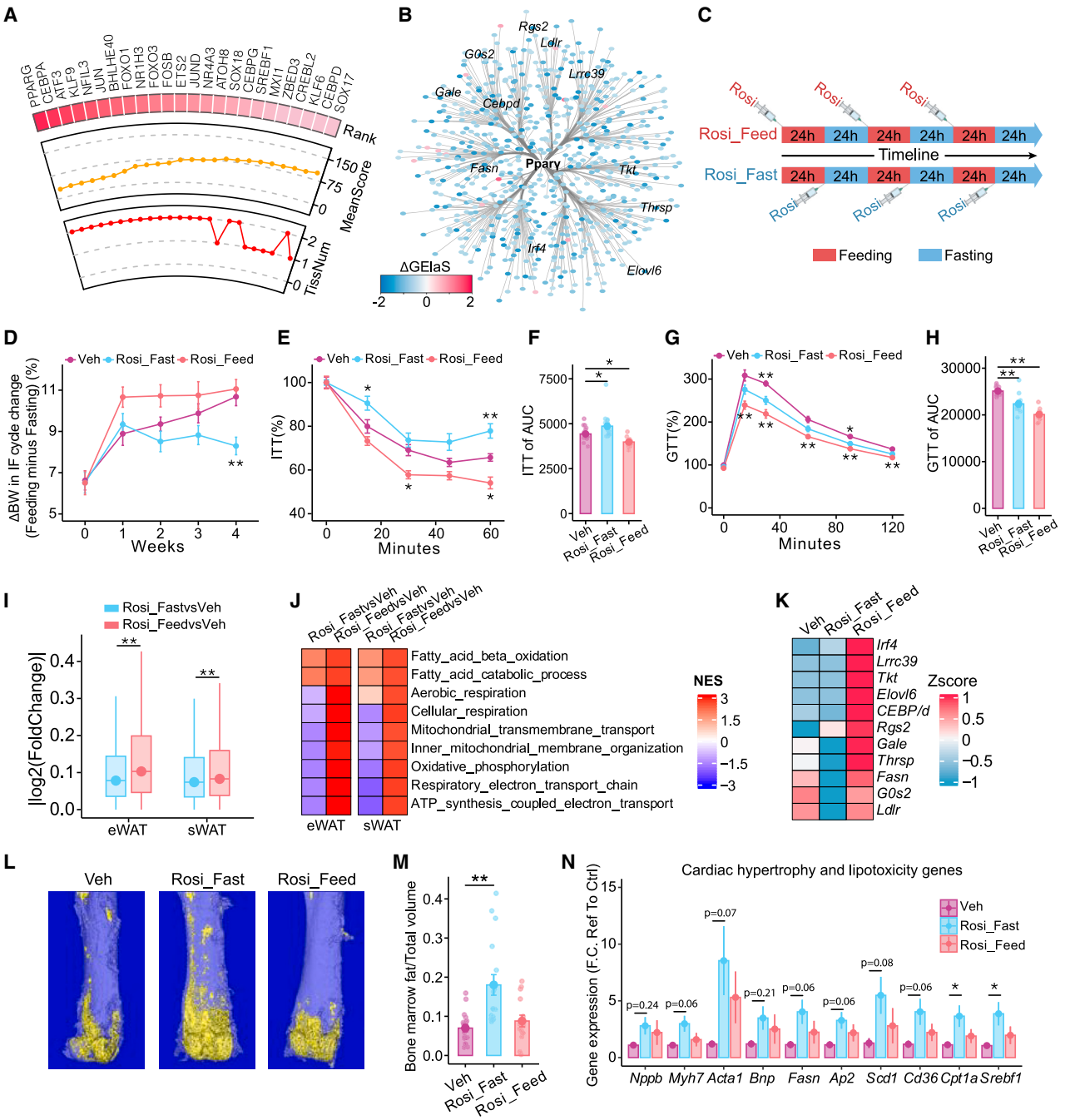

Figure 4. PPARγ agonist treatment in different nutrient status results in distinct metabolic consequences

(A) The TFs enriched in the genes with downregulated GElaS in WAT during aging. The rank is according to the average ranking score (yellow line) between eWAT and sWAT. A smaller score represents a stronger enrichment. The red line indicates the number of tissues where TFs are significantly enriched.

(B) Gene network of PPARγ's target genes. The color indicates the ΔGElaS between the young and aged mice.

(C) A schematic diagram of workflows for Rosi treatment in IF treatment. Aged mice were subjected to IF and Rosi treatment (as described in STAR Methods).

(D) Body weight changes during the treatment. n = 18 (Veh), 18 (Rosi_Fast), and 15/17 (Rosi_Feed). The low asterisk indicates the statistical significance between Rosi_Fast and Veh.

(E) Insulin tolerance test (ITT) for the Veh (n = 17), Rosi_Fast (n = 18), and Rosi_Feed (n = 14) groups. The high and low asterisks indicate the statistical significance for Rosi_Fast versus Veh and Rosi_Feed versus Veh, respectively.

(F) Area under the curve (AUC) of ITT (%).

(G and H) Glucose tolerance test (GTT) and its AUC in the three groups of mice. n = 10/group. The high and low asterisks indicate the statistical significance for Rosi_Fast versus Veh and Rosi_Feed versus Veh, respectively.

(legend continued on next page)

cut-off for differential elastic genes—those whose elasticity varies significantly with age. We identified 1,899, 2,052, 1,302, and 1,155 differential elastic genes in eWAT, sWAT, liver, and muscle, respectively, between young and aged mice (Figure 3D; Table S1). Aging-related changes in gene elasticity are generally tissue specific, but we have found a substantial number of differential elastic genes shared by eWAT and iWAT (Figures S3H–S3K). The majority of differential elastic genes become less elastic during aging (Figure 3D), consistent with the global GElaS changes (Figure 3C). qPCR confirmed the decreased elasticity of some key regulators of carbohydrate and lipid metabolism in eWAT and liver (Figures 3E, 3F, and S3L). Furthermore, pathway analysis of genes with reduced GElaS revealed significant enrichment in lipid, carbohydrate, and sterol metabolism (Figures 3G and S3M–S3O).

Metabolic elasticity is applicable to intermittent fasting and diet challenge

As intermittent fasting (IF) is known to confer a variety of beneficial effects on metabolic health in aging rodents,[16,17] we next investigated the impact of IF on metabolic elasticity. As expected, a 6-week IF treatment was sufficient to reduce body weight and improve insulin sensitivity in aged mice (Figures S4A–S4C), attesting to the success of our IF intervention. Indeed, this IF regimen improved the elasticity of several metabolic parameters, including body weight, fat mass, lean mass, and levels of insulin and lipids (Figures S4A–S4C). These improvements in metabolic elasticity with IF mirror those of gene elasticity, reflected in a generalized increase in metabolic-gene GElaS across adipose tissue and liver (Figures S4D–S4F). Interestingly, glucose elasticity decreased rather than increased following IF (Figures S4A and S4C), due to an IF-associated fall in glucose levels in both AL and R states (Figure S4B), and this change indicates better maintenance of glucose homeostasis. Overall, these data support a role for restoring metabolic elasticity in IF's arrest of aging-related metabolic decline.

The findings presented thus far have been largely derived from alternating fasting-refeeding nutrient challenges. To determine whether metabolic elasticity can be applied to other types of nutrient challenges, we fed 2- and 18-month-old animals a high-fat diet (HFD) for 1 week, followed by 1-week chow diet recovery period (Figure S4G). Body weight, fat mass, insulin, glucose, and FFA levels rose during the weeklong HFD treatment in both young and old mice, but all of these changes reversed after switching back to chow diet (Figure S4H). However, the elasticity of these parameters was higher overall in young mice than in old mice (Figures S4I and S4J). These results suggest that metabolic elasticity can be extended from a feeding-state-based challenge to a diet composition-based challenge, while aging impairs metabolic elasticity under each of these conditions.

Identification of PPARγ as a key regulator of gene elasticity in adipose tissues

Decreases in GElaS during aging suggest dysregulation of the transcriptional response to nutrient fluctuations, in turn implicating transcription factors (TFs). To identify potential transcriptional regulators of metabolic elasticity, we conducted TF-enrichment analysis by ChEA3[18] targeting genes exhibiting decreased elasticity in adipose tissues (Figure 3D). The top candidates include a number of crucial regulators of metabolism and adipogenesis, including C/EBPα, FOXO1, KLF9, and SREBP1 (Figure 4A). Foremost among these is PPARγ, a key coordinator of glucose and lipid metabolism.[19,20] Treatment with thiazolidinedione (TZD) agonists alleviates metabolic dysfunction and extends lifespan in aged mice.[21] Correspondingly, the majority of PPARγ's target genes do exhibit decreased GElaS during aging (Figure 4B), further supporting a role for its dysregulation in the aging-related decline of metabolic elasticity.

If this were the case, optimizing PPARγ activity would enhance GElaS and metabolic health during aging. As PPARγ activity is induced by feeding and repressed by fasting,[22,23] we sought to reinforce its activity at its physiologic peak. To do so, we administered the TZD PPARγ agonist rosiglitazone (Rosi) during the feeding phase of IF in aged animals (Rosi_Feed) (Figure 4C). As a control, we administered Rosi treatment during the fasting phase to perturb the normal cycle of PPARγ activity (Rosi_Fast) (Figure 4C). IF augmented body-weight changes during the fasting/feeding phase switch from approximately 6.5% to 10.5% after a 4-week treatment in the control group, indicating an enhanced metabolic response to IF (Figure 4D). The body-weight changes increased more quickly in the Rosi_Feed group than controls but diminished in the Rosi_Fast group (Figure 4D), indicating a stronger metabolic response in the Rosi_Feed group. The Rosi_Feed treatment concordantly improved insulin sensitivity (Figures 4E and 4F) and glucose tolerance (Figures 4G and 4H), while Rosi_Fast attenuated the drug's ability to improve glucose tolerance and frankly worsened insulin sensitivity.

To assess the transcriptomic effects of these TZD treatment regimens, we compared patterns of gene expression in eWAT and sWAT, where PPARγ is the most abundantly expressed. Rosi_Feed treatment promoted global gene-expression changes more strongly than Rosi_Fast (Figure 4I). Gene set enrichment analysis (GSEA) showed that Rosi_Feed promoted pathways related to mitochondrial metabolism and fatty acid catabolism in adipose tissues, whereas Rosi_Fast blunted or even repressed these gene-expression programs relative to vehicle control (Figure 4J). These data demonstrate that the metabolic consequences of PPARγ activation are dependent on feeding state (Figures 4D–4J), raising the question of whether such feeding-state-dependent

(I) The global gene-expression changes induced by Rosi_Fast and Rosi_Feed treatment in eWAT and sWAT (Mann-Whitney test). The box covers a range of fold changes from 25% (Q1) to 75% (Q3) quantile. The dot in the box indicates the median value of gene-expression changes.
(J) The biological processes influenced by Rosi treatment were analyzed by GSEA (gene set enrichment analysis). The selected pathways are plotted in heatmap. These pathways have a higher NES (normalized enrichment score) in Rosi_Feed group (NES > 2.5 and FDR < 0.05).
(K) The elastic scores of top-changed PPARγ's target genes in eWAT were derived from the qPCR results.
(L) Representative images of bone marrow adiposity of the femurs from the Veh, Rosi_Fast, and Rosi_Feed group mice.
(M) Quantification of bone marrow adiposity in Veh (n = 18), Rosi_Fast (n = 17), and Rosi_Feed (n = 15) groups.
(N) The expression of markers of cardiac hypertrophy and lipotoxicity in the heart of these mice (n = 6). *Rpl23* was used as the reference gene.
Data are shown as mean ± SEM (D–H, M, and N). *p < 0.05, **p < 0.01, one-way ANOVA with Tukey's test (D–H, M, and N) or Mann-Whitney test (I).

effects correlate with alterations in gene elasticity. We selected 11 PPARγ targets based on their ΔGElaS in adipose tissue during aging (Figure 4B) and conducted qPCR in adipose tissue samples from Rosi_Feed and Rosi_Fast groups. As expected, the gene-expression elasticity of examined targets was enhanced in the Rosi_Feed group but not in the Rosi_Fast group (Figure 4K), reinforcing the PPARγ-mediated connection between gene-expression elasticity and metabolic health.

Despite the clear benefits of PPARγ activation, clinical use of TZD agonists has waned, due mainly to their significant adverse effects. Given the feeding dependence of Rosi's metabolic benefits, we likewise considered whether its adverse effects vary with nutrient status. Bone loss figures prominently among the common side effects of TZDs because they tilt the balance of skeletal remodeling toward marrow fat expansion.[24] Although Rosi treatment during the fasting phase significantly increased marrow adiposity, Rosi treatment during the feeding phase did not (Figures 4L and 4M). Cardiac hypertrophy is another major side effect of TZDs, attributed to enhanced expression of pro-hypertrophic genes and genes associated with lipid toxicity.[25,26] We observed upregulation of pro-hypertrophic genes (*Nppb*, *Myh7*, *Acta1*, and *Bnp*) and lipid-metabolic genes (*Fasn*, *Fabp4*, *Scd1*, *Cd36*, *Cpt1a*, and *Srebf1*) predominantly in the hearts of Rosi_Fast mice but not in the Rosi-Feed group (Figure 4N). These data indicate that synchronization of PPARγ agonism with its physiologic activity cycle can improve TZDs' therapeutic index, while dyssynchrony shifts their benefit-to-risk ratio in the opposite direction.

The declines in metabolic elasticity and GElaS are recapitulated in obesity

The results presented earlier have established metabolic elasticity and GElaS as meaningful approaches for manifesting metabolic decline associated with aging. To explore the potential applicability of these concepts to other metabolic conditions, we adopted a diet-induced obesity mouse model. 8 weeks of HFD feeding led to significant increases in body weight and fat mass, along with elevated glucose, insulin, and FFA levels in the bloodstream (Figure S5A). We further evaluated the metabolic plasticity of these parameters in an AL-F-R cycle and, not unexpectedly, observed marked reductions in obese mice (Figures 5A and S5B).

To evaluate the influence of obesity on GElaS, we conducted RNA-seq on eWAT, sWAT, liver, and muscle from chow- and HFD-fed animals (Figure S5C). First, we sought to account for the significant change in adipose tissue cell populations that occurs in obesity, notably including increased immune cell infiltration.[27] We, therefore, asked whether the elastic genes under HFD remained predominantly expressed in adipocytes, as observed in lean mice (Figure 1I), or if their expression became dispersed across different cell types. By comparing the high-GElaS genes with single-nucleus RNA-seq (snRNA-seq) data in HFD-fed mice, we found that genes with high GElaS were still preferentially expressed in adipocytes (Figures 5B and S5D). Importantly, GElaS in HFD samples was significantly lower across all examined organs compared with chow-fed controls (Figure 5C). In line with this observation, the majority of HFD-induced differential elastic genes were down-regulated (Figure 5D; Table S2). The genes with decreased GElaS were predominantly involved in lipid, carbohydrate, and nucleotide metabolism pathways (Figures 5E and S5E–S5G). Collectively, our results demonstrate a significant decline in GElaS in metabolic organs in diet-induced obesity, mirroring the pattern in aging (Figures 3C and 3D).

Given that both aging and obesity lead to decreases in metabolic elasticity and GElaS, we next asked whether these two conditions similarly affected each gene. We observed a generally positive correlation between obesity- and aging-induced GElaS alterations (Figures 5F, 5G, S5H, and S5I). Additionally, the differential elastic genes in HFD-fed mice and aging exhibited significant overlap (Figure S5J). Among the commonly affected genes are many key metabolic regulators, such as *Lep* and *Fasn* in eWAT, *Lep* and *Acaca* in sWAT, *Srebf1* and *Gck* in liver, and *Lpl* and *Hk2* in muscle (Figures 5F, 5G, S5H, and S5I). Thus, GElaS is modulated in a similar manner at the gene level in obesity and aging, underscoring the intertwined nature of these two health challenges.

DISCUSSION

We have developed the term metabolic elasticity to depict animals' ability to switch to an adaptive metabolic state with changes in nutrient availability and then back to the pre-established state when nutrient conditions renormalize. Metabolic elasticity likely arises from similar dynamism in the expression of metabolism-related genes, which we term "gene" or "transcriptome elasticity." These concepts are particularly salient in the context of aging and obesity, as we have discovered similar age- and obesity-related impairments in both metabolic and gene elasticity. We have also developed a system for quantification of gene elasticity using GElaS. Genes with higher GElaS are highly enriched in pathways of lipid and carbohydrate metabolism, but their elasticity wanes with age and obesity. Our findings contrast with existing, purely static transcriptomic studies of aging and obesity in which these metabolic pathways are usually overshadowed by predominant inflammatory pathways.[7,11,12] Overall, our study provides a new angle on metabolic physiology and gene-expression alterations in response to nutrient conditions and highlights an elasticity strategy to curb metabolic dysfunction.

One of the most striking findings in this study is the generalized decrease of gene elasticity in aging and obesity, which raises several further points. First, a decrease in elasticity can result from compromised ability to enter an adaptive state upon nutrition status changes and/or failure to return to the pre-established metabolic state upon nutrient status restoration. To what extent each of these possibilities contributes to elasticity reduction during aging and obesity, and the mechanisms underlying these different patterns, remain to be further explored. Second, there is broad consensus that metabolic flexibility—the ability to adapt to nutritional changes by switching fuel utilization between carbohydrates and fatty acids—is impaired with aging and obesity.[5,28] Although impaired metabolic elasticity and metabolic inflexibility depict two related but distinct aspects of metabolic changes, the causal relationship between them is currently unclear. Third, many earlier studies on transcriptomic changes during aging and obesity—some on quite a large scale[7,8,12,29]—are valuable for having covered a broad range of cell types and aging time

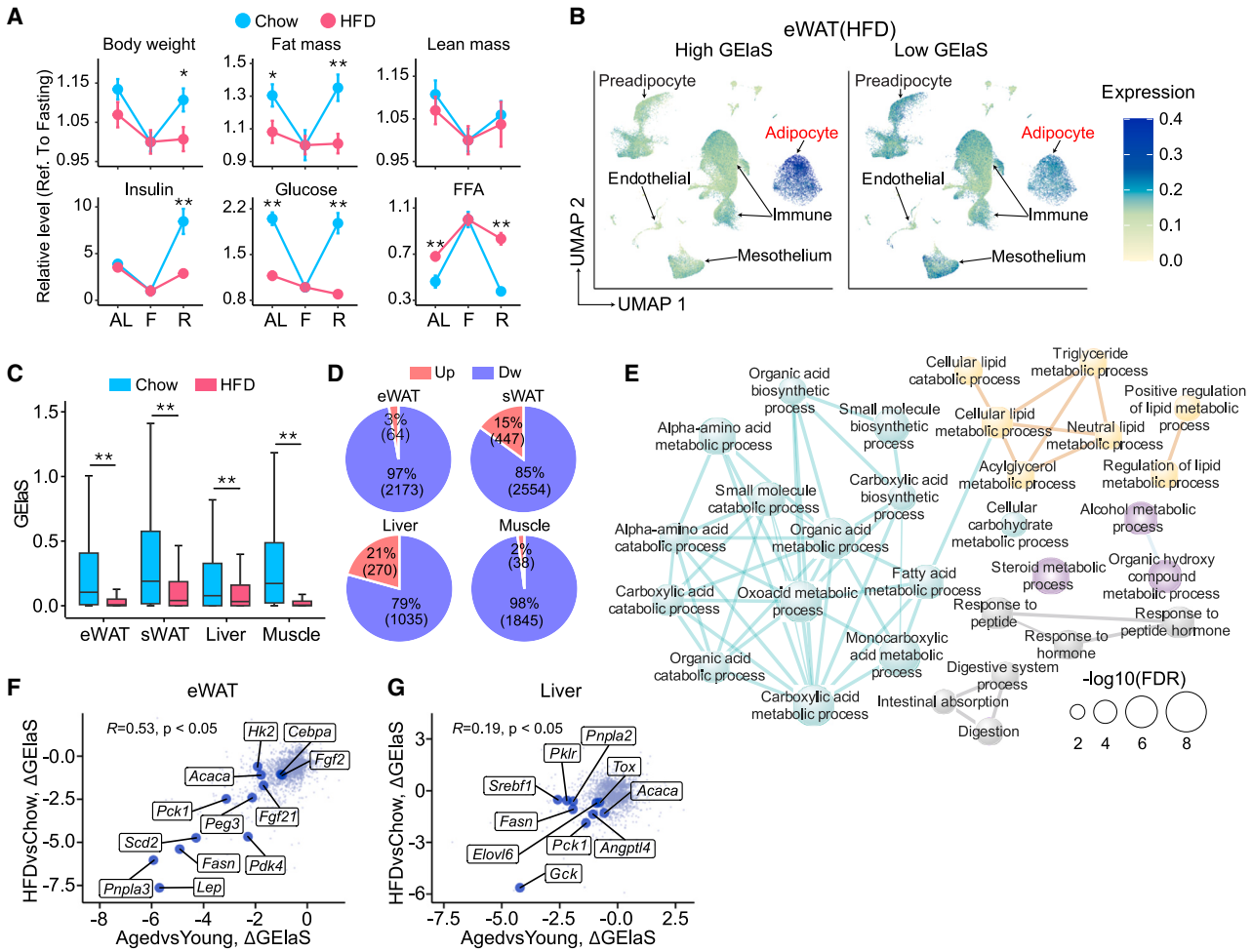

Figure 5. Gene elasticity is impaired during high-fat-diet-induced obesity

(A) The relative values of metabolic parameters including body weight, fat mass, lean mass, insulin, glucose, and FFA in one AL-F-R cycle between chow and high-fat diet mice. The values are normalized to the fasting state of young and aged mice, respectively. Chow, chow diet; HFD, high-fat diet. Data are shown as mean ± SEM (*p < 0.05, **p < 0.01, two-sided Student's t test).

(B) The gene-expression distribution of genes with high (top 500) and low GElaS (bottom 500) across different cell populations in high-fat diet eWAT.

(C) The GElaS distribution in chow and high-fat diet samples. The black line in the box indicates the median value of GElaS. The statistical significance of GElaS average was performed by Mann-Whitney test (*p < 0.05, **p < 0.01).

(D) The number of genes with up- and downregulated GElaS between chow and high-fat diet samples. Up, upregulated gene; Dw, downregulated gene.

(E) Functional enrichment (top 30) for the differential elastic genes with decreased GElaS during high-fat diet (eWAT).

(F and G) Scatterplot for ΔGElaS of AgedvsYoung and HFDvsChow in (F) eWAT and (G) Liver. x axis is the ΔGElaS for AgedvsYoung, while y axis represents the ΔGElaS for HFDvsChow. The correlation analysis was conducted by Pearson's correlation.

points. Unfortunately, most, if not all, of these studies have focused on a single metabolic state, such as *ad libitum* or fasting. Failure to take into account feeding-state dynamics underestimates the complexity of metabolic changes in aging and obesity, favoring a dynamic and elastic interpretation of the transcriptomic alterations in place of traditional static analyses.

Although GElaS often correlates with metabolic elasticity, we do not intend to imply a direct causal relationship between tissue-specific GElaS and systemic metabolic elasticity. GElaS describes changes at the transcriptome level in certain examined tissues. It is conceivable that gene elasticity may exert pleiotropic effects on metabolic health. However, changes in gene elasticity may not directly translate into altered metabolic elasticity, as metabolic elasticity, conveyed by different metabolic parameters, can be influenced by various factors at the systemic and local levels. Furthermore, the same gene often shows different GElaS alterations in different organs (Figures S3H–S3K) because its expression regulation can be heavily influenced by distinct cellular environments. As such, establishing general causal connections between GElaS of specific genes in a particular organ and particular aspects of metabolic elasticity remains challenging.

Our work puts forth an innovative concept—metabolic elasticity—to describe the dynamic nature of metabolic processes required for maintaining energy homeostasis during environmental fluctuations. Further, we have developed GElaS to depict

the elasticity of gene expression that underlies metabolic elasticity. These concepts have enabled us to reveal aging- and obesity-induced declines in elasticity at both the physiological and transcriptomic levels. We foresee this concept of elasticity, approached using GElaS, extending to conditions beyond aging and obesity, including diabetes, exercise, cancer, and many others. We expect that all of these conditions can be reframed as dynamic and elastic processes rather than solely as snapshots of single metabolic states or transitions.

Limitations of the study

In our study, we have established an elasticity score system to quantify changes in metabolic and gene elasticity associated with aging and obesity. However, manipulating the GElaS of a particular gene to investigate its specific influence on metabolic health still presents a significant challenge for the field. Although the gene elasticity profile has been provided for the major metabolic organs during aging and obesity, the protein and metabolite elasticity have not been evaluated, and how they change is still unknown in aging and obesity. The datasets are generated from the male animals, which limits the observation for the female animals. Moreover, having human metabolic and gene elasticity data would provide more information for clinical medicine.

STAR★METHODS

Detailed methods are provided in the online version of this paper and include the following:

SUPPLEMENTAL INFORMATION

Supplemental information can be found online at https://doi.org/10.1016/j.cmet.2023.08.001.

ACKNOWLEDGMENTS

This work was supported by National Institutes of Health R01DK112943 (L.Q.), R01DK128848 (L.Q.), R01DK131169 (L.Q.), and P01 HL087123 (L.Q.) and the Russell Berrie Foundation (L.Q.). This work was also supported by National Medical Research Council Singapore MOH-000954 (L.S.), MOH-000379 (L.S.), NMRC/OFIRG/0062/2017 (L.S.), Ministry of Education MOE2019-T2-1-025 (L.S.), and National Medical Research Council Singapore MOH-000657 (Q.Z.). We also thank Dr. Yen Ching Lim for technical support.

AUTHOR CONTRIBUTIONS

L.Q. and L.S. conceived, designed, and supervised the study. L.Y. performed the experiments and Q.Z. performed the sequencing analyses. J.R.C. contributed to data discussion, concept development, and manuscript editing. All the authors analyzed the data and wrote the manuscript.

DECLARATION OF INTERESTS

The authors declare no competing interests.

INCLUSION AND DIVERSITY

We support inclusive, diverse, and equitable conduct of research.

Received: October 5, 2022
Revised: May 4, 2023
Accepted: August 1, 2023
Published: August 24, 2023

REFERENCES

1. Barzilai, N., Huffman, D.M., Muzumdar, R.H., and Bartke, A. (2012). The critical role of metabolic pathways in aging. Diabetes *61*, 1315–1322.
2. Smith, H.J., Sharma, A., and Mair, W.B. (2020). Metabolic communication and healthy aging: where should we focus our energy? Dev. Cell *54*, 196–211.
3. López-Otín, C., Blasco, M.A., Partridge, L., Serrano, M., and Kroemer, G. (2013). The hallmarks of aging. Cell *153*, 1194–1217.
4. Goodpaster, B.H., and Sparks, L.M. (2017). Metabolic flexibility in health and disease. Cell Metab. *25*, 1027–1036.
5. Riera, C.E., and Dillin, A. (2015). Tipping the metabolic scales towards increased longevity in mammals. Nat. Cell Biol. *17*, 196–203.
6. Sakers, A., De Siqueira, M.K., Seale, P., and Villanueva, C.J. (2022). Adipose-tissue plasticity in health and disease. Cell *185*, 419–446.
7. Tabula Muris Consortium (2020). A single-cell transcriptomic atlas characterizes ageing tissues in the mouse. Nature *583*, 590–595.
8. Emont, M.P., Jacobs, C., Essene, A.L., Pant, D., Tenen, D., Colleluori, G., Di Vincenzo, A., Jørgensen, A.M., Dashti, H., Stefek, A., et al. (2022). A single-cell atlas of human and mouse white adipose tissue. Nature *603*, 926–933.
9. The Tabula Muris Consortium; Overall coordination; Logistical coordination; Organ collection and processing; Library preparation and sequencing; Computational data analysis; Cell type annotation; Writing group; Supplemental text writing group; Principal investigators (2018).

Single-cell transcriptomics of 20 mouse organs creates a *Tabula Muris*. Nature *562*, 367–372.

10. Han, L., Wei, X., Liu, C., Volpe, G., Zhuang, Z., Zou, X., Wang, Z., Pan, T., Yuan, Y., Zhang, X., et al. (2022). Cell transcriptomic atlas of the non-human primate *Macaca fascicularis*. Nature *604*, 723–731.
11. Zhou, Q., Wan, Q., Jiang, Y., Liu, J., Qiang, L., and Sun, L. (2020). A landscape of murine long non-coding RNAs reveals the leading transcriptome alterations in adipose tissue during aging. Cell Rep. *31*, 107694.
12. Schaum, N., Lehallier, B., Hahn, O., Pálovics, R., Hosseinzadeh, S., Lee, S.E., Sit, R., Lee, D.P., Losada, P.M., Zardeneta, M.E., et al. (2020). Ageing hallmarks exhibit organ-specific temporal signatures. Nature *583*, 596–602.
13. Buniello, A., MacArthur, J.A.L., Cerezo, M., Harris, L.W., Hayhurst, J., Malangone, C., McMahon, A., Morales, J., Mountjoy, E., Sollis, E., et al. (2019). The NHGRI-EBI GWAS Catalog of published genome-wide association studies, targeted arrays and summary statistics 2019. Nucleic Acids Res. *47*, D1005–D1012.
14. Calçada, D., Vianello, D., Giampieri, E., Sala, C., Castellani, G., de Graaf, A., Kremer, B., van Ommen, B., Feskens, E., Santoro, A., et al. (2014). The role of low-grade inflammation and metabolic flexibility in aging and nutritional modulation thereof: a systems biology approach. Mech. Ageing Dev. *136–137*, 138–147.
15. Finkel, T. (2015). The metabolic regulation of aging. Nat. Med. *21*, 1416–1423.
16. de Cabo, R., and Mattson, M.P. (2019). Effects of intermittent fasting on health, aging, and disease. N. Engl. J. Med. *381*, 2541–2551.
17. Mattson, M.P., Longo, V.D., and Harvie, M. (2017). Impact of intermittent fasting on health and disease processes. Ageing Res. Rev. *39*, 46–58.
18. Keenan, A.B., Torre, D., Lachmann, A., Leong, A.K., Wojciechowicz, M.L., Utti, V., Jagodnik, K.M., Kropiwnicki, E., Wang, Z., and Ma'ayan, A. (2019). ChEA3: transcription factor enrichment analysis by orthogonal omics integration. Nucleic Acids Res. *47*, W212–W224.
19. Lefterova, M.I., Haakonsson, A.K., Lazar, M.A., and Mandrup, S. (2014). PPARgamma and the global map of adipogenesis and beyond. Trends Endocrinol. Metab. *25*, 293–302.
20. Montaigne, D., Butruille, L., and Staels, B. (2021). PPAR control of metabolism and cardiovascular functions. Nat. Rev. Cardiol. *18*, 809–823.
21. Xu, L., Ma, X., Verma, N., Perie, L., Pendse, J., Shamloo, S., Marie Josephson, A., Wang, D., Qiu, J., Guo, M., et al. (2020). PPARgamma agonists delay age-associated metabolic disease and extend longevity. Aging Cell *19*, e13267.
22. Dubois, V., Eeckhoute, J., Lefebvre, P., and Staels, B. (2017). Distinct but complementary contributions of PPAR isotypes to energy homeostasis. J. Clin. Invest. *127*, 1202–1214.
23. Vidal-Puig, A., Jimenez-Liñan, M., Lowell, B.B., Hamann, A., Hu, E., Spiegelman, B., Flier, J.S., and Moller, D.E. (1996). Regulation of PPAR gamma gene expression by nutrition and obesity in rodents. J. Clin. Invest. *97*, 2553–2561.
24. Wei, W., and Wan, Y. (2011). Thiazolidinediones on PPARγ: the roles in bone remodeling. PPAR Res. *2011*, 867180.
25. Son, N.H., Park, T.S., Yamashita, H., Yokoyama, M., Huggins, L.A., Okajima, K., Homma, S., Szabolcs, M.J., Huang, L.S., and Goldberg, I.J. (2007). Cardiomyocyte expression of PPARgamma leads to cardiac dysfunction in mice. J. Clin. Invest. *117*, 2791–2801.
26. Nissen, S.E., and Wolski, K. (2007). Effect of rosiglitazone on the risk of myocardial infarction and death from cardiovascular causes. N. Engl. J. Med. *356*, 2457–2471.
27. Fuster, J.J., Ouchi, N., Gokce, N., and Walsh, K. (2016). Obesity-induced changes in adipose tissue microenvironment and their impact on cardiovascular disease. Circ. Res. *118*, 1786–1807.
28. Smith, R.L., Soeters, M.R., Wüst, R.C.I., and Houtkooper, R.H. (2018). Metabolic flexibility as an adaptation to energy resources and requirements in health and disease. Endocr. Rev. *39*, 489–517.
29. Sárvári, A.K., Van Hauwaert, E.L., Markussen, L.K., Gammelmark, E., Marcher, A.B., Ebbesen, M.F., Nielsen, R., Brewer, J.R., Madsen, J.G.S., and Mandrup, S. (2021). Plasticity of epididymal adipose tissue in response to diet-induced obesity at single-nucleus resolution. Cell Metab. *33*, 437–453.e5.
30. Andrews, S. (2010). FastQC: a quality control tool for high throughput sequence data. http://www.bioinformatics.babraham.ac.uk/projects/fastqc.
31. Dobin, A., Davis, C.A., Schlesinger, F., Drenkow, J., Zaleski, C., Jha, S., Batut, P., Chaisson, M., and Gingeras, T.R. (2013). STAR: ultrafast universal RNA-seq aligner. Bioinformatics *29*, 15–21.
32. Liao, Y., Smyth, G.K., and Shi, W. (2014). featureCounts: an efficient general purpose program for assigning sequence reads to genomic features. Bioinformatics *30*, 923–930.
33. Dowle, M., and Srinivasan, A. (2021). data.table: extension of data.frame. https://github.com/Rdatatable/data.table.
34. Ritchie, M.E., Phipson, B., Wu, D., Hu, Y., Law, C.W., Shi, W., and Smyth, G.K. (2015). limma powers differential expression analyses for RNA-sequencing and microarray studies. Nucleic Acids Res. *43*, e47.
35. Kolberg, L., Raudvere, U., Kuzmin, I., Vilo, J., and Peterson, H. (2020). gprofiler2 – an R package for gene list functional enrichment analysis and namespace conversion toolset g:Profiler. F1000Res *9*, ELIXIR-709.
36. Merico, D., Isserlin, R., Stueker, O., Emili, A., and Bader, G.D. (2010). Enrichment map: a network-based method for gene-set enrichment visualization and interpretation. PLoS One *5*, e13984.
37. Shannon, P., Markiel, A., Ozier, O., Baliga, N.S., Wang, J.T., Ramage, D., Amin, N., Schwikowski, B., and Ideker, T. (2003). Cytoscape: a software environment for integrated models of biomolecular interaction networks. Genome Res. *13*, 2498–2504.
38. Subramanian, A., Tamayo, P., Mootha, V.K., Mukherjee, S., Ebert, B.L., Gillette, M.A., Paulovich, A., Pomeroy, S.L., Golub, T.R., Lander, E.S., et al. (2005). Gene set enrichment analysis: a knowledge-based approach for interpreting genome-wide expression profiles. Proc. Natl. Acad. Sci. USA *102*, 15545–15550.
39. Hao, Y., Hao, S., Andersen-Nissen, E., Mauck, W.M., 3rd, Zheng, S., Butler, A., Lee, M.J., Wilk, A.J., Darby, C., Zager, M., et al. (2021). Integrated analysis of multimodal single-cell data. Cell *184*, 3573–3587.e29.
40. Bengtsson, H. (2021). matrixStats: functions that apply to rows and columns of matrices (and to vectors). R package version: 0.58.0. https://CRAN.R-project.org/package=matrixStats.
41. Koncevičius, K. (2020). Fast statistical hypothesis tests on rows and columns of matrices. R package version: 0.1.9. https://github.com/KKPMW/matrixTests.
42. Constantin, A.-E., and Patil, I. (2021). R package for displaying significance brackets. https://const-ae.github.io/ggsignif/.
43. Wickham, H. (2016). ggplot2: Elegant Graphics for Data Analysis (Springer-Verlag).
44. Gu, Z., Eils, R., and Schlesner, M. (2016). Complex heatmaps reveal patterns and correlations in multidimensional genomic data. Bioinformatics *32*, 2847–2849.
45. Frankish, A., Diekhans, M., Ferreira, A.M., Johnson, R., Jungreis, I., Loveland, J., Mudge, J.M., Sisu, C., Wright, J., Armstrong, J., et al. (2019). GENCODE reference annotation for the human and mouse genomes. Nucleic Acids Res. *47*, D766–D773.
46. Ardlie, K.G., DeLuca, D.S., Segre, A.V., Sullivan, T.J., Young, T.R., Gelfand, E.T., Trowbridge, C.A., Maller, J.B., Tukiainen, T., and Lek, M. (2015). Human genomics. The Genotype-Tissue Expression (GTEx) pilot analysis: multitissue gene regulation in humans. Science *348*, 648–660.

STAR★METHODS

KEY RESOURCES TABLE

REAGENT or RESOURCE	SOURCE	IDENTIFIER
Biological samples		
Crab-eating macaques (*Macaca fascicularis*): visceral (omental) white adipose	HuaZheng Laboratory Animal Breeding Centre	N/A
Crab-eating macaques (*Macaca fascicularis*): subcutaneous white adipose	HuaZheng Laboratory Animal Breeding Centre	N/A
Crab-eating macaques (*Macaca fascicularis*): liver	HuaZheng Laboratory Animal Breeding Centre	N/A
Crab-eating macaques (*Macaca fascicularis*): muscle	HuaZheng Laboratory Animal Breeding Centre	N/A
Chemicals, peptides, and recombinant proteins		
Rosiglitazone	Abcam	Ab12461
Trizol	Sigma	T9424
NucleoSpin RNA Set for NucleoZOL	Macherey-Nagel	740406
High-Capacity cDNA Reverse Transcription Kit	Applied Biosystems (Fisher Scientific)	43-688-14
AzuraView GreenFast qPCR Blue Mix LR	Azura Genomics	50737RC103
Deposited data		
RNA-seq data for eWAT, sWAT, liver, and muscle during the AL-F-R cycle in young and aged mice	This paper	NGDC (https://ngdc.cncb.ac.cn): CRA008068.
RNA-seq data for the biopsies from liver, muscle, subcutaneous and visceral (omental) white adipose tissues in Crab-eating macaques (*Macaca fascicularis*) during the AL-F-R cycle	This paper	NGDC (https://ngdc.cncb.ac.cn): CRA008075.
RNA-seq data for the Rosi-treatment	This paper	NGDC (https://ngdc.cncb.ac.cn): CRA008081.
RNA-seq data for eWAT, sWAT, liver, and muscle during the AL-F-R cycle in chow and high-fat diet mice	This paper	NGDC (https://ngdc.cncb.ac.cn): CRA010713.
Mouse reference genome (GRCm39)	GENCODE	https://www.gencodegenes.org
Crab-eating macaques reference genome (v6.0)	Ensembl	https://www.ensembl.org
Single nuclei RNA-seq dataset for eWAT and sWAT in mouse	Emont et al.[8]	https://singlecell.broadinstitute.org/single_cell/study/SCP1376/a-single-cell-atlas-of-human-and-mouse-white-adipose-tissue
Single cell RNA-seq dataset for Liver in mouse	Tabula Muris Consortium	https://github.com/czbiohub-sf/tabula-muris
Single nuclei RNA-seq dataset for Crab-eating macaques	Han et al.[10]	https://db.cngb.org/nhpca
Experimental models: Organisms/strains		
Mouse (C57BL/6J)	The Jackson Laboratory	https://www.jax.org
Crab-eating macaques (*Macaca fascicularis*)	HuaZheng Laboratory Animal Breeding Centre	N/A
Oligonucleotides		
Primers for this paper, see Table S3	This paper	N/A

(*Continued on next page*)

Continued

REAGENT or RESOURCE	SOURCE	IDENTIFIER
Software and algorithms		
Quality control of RNA-seq: fastqc v0.11.9	Andrews[30]	http://www.bioinformatics.babraham.ac.uk/projects/fastqc
RNA-seq Mapping: STAR v2.7.7a	Dobin et al.[31]	https://github.com/alexdobin/STAR
Counting reads: featureCounts v2.0.1	Liao et al.[32]	http://subread.sourceforge.net
R system: R v4.0.2	R Core Team	https://cran.r-project.org
Programming environment of R: RStudio v1.4.1103	RStudio Team	https://www.rstudio.com
Input/Output data: data.table v1.14.3	Dowle and Srinivasan[33]	https://github.com/Rdatatable/data.table
Gene expression analysis: limma v3.44.3	Ritchie et al.[34]	https://bioconductor.org/packages/release/bioc/html/limma.html
Functional enrichment analysis: gprofiler2 (v0.2.0)	Kolberg et al.[35]	https://cran.r-project.org/web/packages/gprofiler2/vignettes/gprofiler2.html
Functional enrichment visualization: EnrichmentMap v3.3.2	Merico et al.[36]	https://apps.cytoscape.org/apps/enrichmentmap
Cytoscape	Shannon et al.[37]	https://cytoscape.org
Gene Set Enrichment Analysis (GSEA v4.0)	Subramanian et al.[38]	https://www.gsea-msigdb.org/gsea/index.jsp
TF enrichment analysis: ChEA3	Keenan et al.[18]	https://maayanlab.cloud/chea3
Single-cell analysis: Seurat v4.0.4	Hao et al.[39]	https://satijalab.org/seurat
Matrix analysis: matrixStats v0.58.0	Bengtsson[40]	https://CRAN.R-project.org/package=matrixStats
Statistical analysis for matrix: matrixTests v0.1.9	Koncevičius[41]	https://github.com/KKPMW/matrixTests
Statistical analysis: ggsignif v0.6.1	Constantin and Patil[42]	https://const-ae.github.io/ggsignif
Data visualization: ggplot2 v3.3.3	Wickham[43]	https://ggplot2.tidyverse.org
Data visualization: ComplexHeatmap v2.7.6.1010	Gu et al.[44]	https://github.com/jokergoo/ComplexHeatmap
Quantum FX μCT Scanner	Perkin-Elmer	CLS149276
Analyze 12.0	Analyze Direct	N/A
Bio-rad CFX Conect, Real-Time system	Bio-rad	N/A
Bio-rad CFX Manager	CFX Manager 3.1	N/A

RESOURCE AVAILABILITY

Lead contact

Further information and requests for resources and reagents should be directed to the lead contact, Dr. Lei Sun (sun.lei@duke-nus.edu.sg).

Materials availability

This study did not generate unique reagents.

Data and code availability

The computer core code used for the data analysis in this paper is available at GitHub (https://github.com/zhouqz/GElaS). The RNA-seq data for eWAT, sWAT, liver, and muscle during the AL-F-R cycle in young and aged mice are available at NGDC (https://ngdc.cncb.ac.cn/): CRA008068. The RNA-seq data for the biopsies from liver, muscle, subcutaneous and visceral (omental) white adipose tissues in Crab-eating macaques during the AL-F-R cycle are available at NGDC (https://ngdc.cncb.ac.cn/): CRA008075. The RNA-seq data for the Rosi-treatment is available at NGDC (https://ngdc.cncb.ac.cn/): CRA008081. The RNA-seq data for eWAT, sWAT, liver, and muscle during the AL-F-R cycle in chow and HFD mice are available at NGDC (https://ngdc.cncb.ac.cn/): CRA010713. The values used to generate graphs are available in Data S1. All other relevant materials and data supporting the major findings of this study are provided in the article and its additional information files and are also available from the corresponding author on reasonable request.

EXPERIMENTAL MODEL AND STUDY PARTICIPANT DETAILS

Animals

All mice (male, 2-18 months) were on C57BL/6J background and maintained under standard laboratory conditions with standard chow diet (PicoLab rodent diet 20, 5053; Purina Mills). Mice were housed on a 12-hour light/dark cycle with free access to food and water at an ambient temperature of 23 ± 1°C. The health status checks were conducted regularly in the animal breeding facility. All animal experiments were performed in accordance with NIH guidelines for Animal Care and Use, approved and overseen by Columbia University Institutional Animal Care and Use Committee (IACUC).

For glucose tolerance test (GTT), mice were fasted overnight for 16 hr (5 p.m. to 9 a.m.) and intraperitoneally injected with glucose at a dose of 2 g/kg•BW. Blood glucose levels were measured at basal state (0 min) and then at 15, 30, 60, 90, and 120 minutes after injection. Insulin tolerance test (ITT) was performed after a 4-hr (9 a.m. to 1 p.m.) fasting period through the intraperitoneal injection of human insulin (0.75 U/kg•BW). Blood glucose levels were measured at the indicated times via tail vein bleeding using OneTouch glucometer. We used Infinity Triglyceride Reagent (Thermo Scientific) and NEFA-HR (Fujifilm Wako) to measure plasma triglyceride and FFA levels, respectively. Plasma insulin was measured using Insulin ELISA kit (Mercodia).

All experiments involving non-human primates in this study were reviewed and approved by the Institutional Animal Care and Use Committee of HuaZheng Laboratory Animal Breeding Centre. The non-human primates (*Macaca fascicularis*, male, 9.4-20.3 years old) were housed in the animal facilitates in HuaZheng Laboratory Animal Breeding Centre and maintained on a regular 12-hour light/dark cycle with an ambient temperature of 18∼26 °C. Each monkey was fed with unlimited food for a specific duration (30 minutes) twice a day, once in the morning and once in the evening. Additionally, 150 g of fruit was provided between meals, also for a specific period of time (30 minutes). The veterinarian performed two daily health status checks in the animal facilities regularly.

METHOD DETAILS

RNA extraction and Real-Time PCR

Young (2 months) and aged (18 months) animals were sacrificed at *ad libitum*, fasting (16 hours), and refeeding (4 hours food access after 16 hours fasting) states to harvest the liver, gastrocnemius muscle, epididymal adipose tissue (eWAT) and inguinal adipose tissues (sWAT) from the animals at *ad libitum*, fasting, and refeeding states, separately. The animals began fasting at 5:00 -6:00 pm in the AL-F-R cycle. Tissues were lysed with TriZol reagent (Thermo Fisher). After phase separation through the addition of chloroform, RNA was isolated using the NucleoSpin RNA kit (Macherey-Nagel). cDNA was synthesized from 1 μg total RNA by using the High-capacity cDNA Reverse Transcription kit (Applied Biosystems). Quantitative real-time PCR (qPCR) was performed on a Bio-Rad CFX96 Real-Time PCR system using the GoTaq qPCR Master Mix (Promega). Relative gene expression levels were calculated using the ΔΔCt method with Rpl23 or Cyclophilin A as the reference gene. The primer sequences are provided in Table S3.

RNA sequencing

The strand-specific RNA-seq libraries were prepared and sequenced by Novogene. The quality of RNAs and libraries were examined with Agilent 2100. RNA-seq libraries were multiplexed and RNA sequencing were performed using the Illumina's NovaSeq 6000 platform. FastQC (v0.11.9) was used for the quality control of RNA-seq data.[30]

The calculation of gene expression elasticity

The RNA-seq data were mapped to the mouse genome (GRCm39) using STAR (2.7.7a), and featureCounts (v2.0.1) was employed to compute the read counts for each gene in each sample.[31,32,45] Then we employed limma (v3.44.3) to conduct the differentially expressed analysis.[34] The read counts were normalized by the TMM (Trimmed Mean of M-values) method and converted to the gene expression (FPKM, fragments per kilobase per million). The Gene Elastic Score (GElaS) was calculated as:

$$\mathrm{GElaS} = Sign * \left(\left|log_2\, FC_{FvsAL}\right| * FDR_{FvsALweight} + \left|log_2\, FC_{RvsF}\right| * FDR_{RvsFweight}\right) * Ratio$$

$$\text{Here}: Sign = \begin{cases} 1 & \left(log_2\, FC_{FvsAL} * log_2\, FC_{RvsF}\right) < 0 \\ 0 & \left(log_2\, FC_{FvsAL} * log_2\, FC_{RvsF}\right) \geq 0 \end{cases}$$

$$Ratio = \min\left(\left|log_2\, FC_{FvsAL}\right|, \left|log_2\, FC_{RvsF}\right|\right) / \max\left(\left|log_2\, FC_{FvsAL}\right|, \left|log_2\, FC_{RvsF}\right|\right)$$

$$FDR_{weight} = \begin{cases} 1 & FDR < 0.05 \\ log\ 10(FDR)/log\ 10(0.05) & FDR \geq 0.05 \end{cases}$$

Here, Log_2FC is log_2FoldChange of gene expression. During the FoldChange calculation, each FPKM value will increase by 0.5 to avoid number zero in log-transformed. FvsAL is Fasting *vs. Ad libitum*, while RvsF represents Refeeding *vs.* Fasting. FDR is False

Discovery Rate. Ratio indicates the restorability. For metabolic parameters and Real-Time PCR data, p-value was used instead of the FDR to calculate the elastic score.

Analyzing the relationship between GElaS and gene expression dynamics, restorability, statistical significance

To check the relationship between GElaS and gene expression dynamics, genes were ranked according to their GElaS and selected the high GElaS group (top 500 genes) and the low GElaS group (bottom 500 genes). The gene expression fold changes upon fasting and refeeding were compared between the high- and low-GElaS groups (Figure 1D). Moreover, the Spearman correlation analysis was conducted to investigate the relationship between the GElaS and gene expression dynamics (fold changes upon fasting and refeeding), restorability (Ratio in the formula above), statistical significance (Figure S1D), separately.

Functional enrichment analysis of sliding windows

A sliding window approach was applied to check the functional relevance of GElaS. Genes were ranked according to their GElaS and subjected to Gene Ontology (biological process category) analysis using gprofiler2 (v0.2.0)[35] in a 500-genes window sliding with 100-genes step length across the GElaS rank (Figures 1F and 2D). The GO biological pathways were filtered out with query genes < 4, background genes > 1000, or background genes < 15. Benjamini–Hochberg method was used to adjust the p-value and remained the GO biological pathway with a criterion of adjusted p-value < 0.1.

The distribution of elastic and non-elastic genes across different cell types in tissues

The single-nucleus RNA-seq (snRNA-seq) of adipose tissue and single-cell RNA-seq (scRNA-seq) of liver were used to investigate the gene expression distribution of the high-(top 500) and low- (bottom 500) GElaS genes in different cell types.[8,9] The gene expression of snRNA-seq and scRNA-seq from the previous studies were averaged for elastic (top-500) and non-elastic (bottom 500) genes in each cell type.[8,9] The 2D UMAP (Uniform Manifold Approximation and Projection) plot was employed to display the expression distribution of elastic and non-elastic genes across different cell types (Figure 1I).

GElaS analysis in non-human primates

The non-human primate experiments were approved and overseen by Institutional Animal Care and Use Committee (IACUC) of HuaZheng Laboratory Animal Breeding Centre. Animals were anesthetized with ketamine hydrochloride (10-20mg/kg) and pentobarbital sodium (8-15mg/kg) and biopsies were taken from liver, muscle, subcutaneous and visceral (omental) white adipose tissues (sWAT and vWAT). For biopsies at *ad libitum*, a cohort of 12 adult Crab-eating macaques (*Macaca fascicularis*, 9.4-20.3 years old) were included in this study. After the biopsy procedure, animals will rest at least 3 weeks to recover before next procedure. For fasting biopsies harvest, animals were fasted for 24 hours with water access and taken biopsies, followed by another 3-weeks rest. The animals started the fasting at 10:00 am after breakfast. For refeeding biopsies, animals were fasted for 24 hours and then fed for 6 hours before biopsy harvest.

We conducted the RNA sequencing for the harvest biopsies. We mapped the RNA-seq data to the Crab-eating macaque genome (*Macaca fascicularis* v6.0) using STAR (2.7.7a)[31] and calculated the read counts for each gene across the samples using featureCounts (v2.0.1).[32] We performed the paired RNA-seq analysis based on the read counts by limma (v3.44.3),[34] followed by GElaS analysis as described above. To examine the cross-species correlation of GElaS between mice and monkeys, we obtained the orthologous genes between Crab-eating macaque and mouse from biomart (https://www.ensembl.org/biomart/martview) and compared the GElaS for elastic genes (GElaS > 0.5 in both species). The single nuclei RNA-seq data was used to examine the cell type distribution between high (top 500) and low (bottom 500)-elastic genes in the non-human primate *Macaca fascicularis*.[10]

The influence of aging on the expression of elastic genes

The aging-regulated genes (AR-genes) list and gene expression in each tissue at different age points were obtained from the previous study.[11] The aging-regulated genes for humans were identified using the method described previously.[11] The gene expression data of human tissues at different ages were from GTEx.[46] The individuals from 50-59 and 60-79 years (50_59Y and 60_79Y) were regarded as the aged samples while the ones from 20-29 years (20_29Y) were marked as the young samples. The gene differentially expressed between (50_59Y *vs.* 20_29Y) or (60_79Y *vs.* 20_29Y) was defined as the AR-gene of human. If a gene showed opposite directional changes in these two comparisons, it was excluded from AR-gene list. The AR-genes number and aging-induced expression changes were calculated in a 500-genes width window sliding across the GElaS rank with 100-genes step length. The numbers of AR-genes and the medium value of aging-induced fold changes in each window were plotted across the GElaS rank. The standard deviation of expression across all aging points (8, 26, 60, 78, 104-weeks) was used to evaluate the expression dynamic across the aging course from 8- to 104-week-old.

The connection between gene elasticity and aging traits in humans

In an expression-independent analysis, the genes containing aging traits-associated SNPs were identified using the GWAS (Genome-Wide Association Study) data (v1.0.2-associations_e104_r2021-09-23) from GWAS Catalog.[13] A gene was categorized as aging associated if its genomic region contains any SNP linked to aging traits (“aging”, “cognition, aging”, “healthspan”, “hippocampal sclerosis of aging”, “longevity”, “longevity, aging”, “longevity, healthspan, parental longevity”, “parental longevity”, and “skin aging measurement”). The orthologous genes between mouse and human were obtained from biomart (https://www.

ensembl.org/biomart/martview) and matched from mouse to human. The number of genes containing aging traits-associated SNPs in the elastic (top 1500) *vs.* non-elastic (bottom 1500) groups were compared to examine if gene elasticity is connected aging traits.

Identification of differential elastic genes between the young and aged mice

The genes were applied a cutoff of $|GElaS_{Aged} - GElaS_{Young}| = |\Delta GElaS| > 0.5$ to identify the differential elastic genes between the young and aging mice. The biological pathway analysis of differential elastic genes was performed using gprofiler2 (v0.2.0).[35] The connection between the biological pathways was conducted using EnrichmentMap[36] (Figure 3G).

Intermittent fasting and Rosiglitazone treatment

16-mon-old male C57BL/6J mice were subjected to 24-hour intermittent fasting starting at 5-6 pm every day for 6 weeks. Animals were monitored for weight changes and body mass. GTT was performed at 5 weeks of IF after 24hr fasting, and ITT was performed at 5 weeks of IF after 4-hr fasting during the feeding phase. The temporal feeding behavior data during intermittent fasting were recorded (Table S4). Rosi (Rosiglitazone) (5 mg/kg·W) were given intraperitoneally to IF mice at a dosage of 5 mg/kg in every IF cycle during the fasting (Rosi-Fast) or feeding phase (Rosi-Feed). We administered Rosi at a consistent time (5-6 pm, within 1-2 hours prior to light off) for both Rosi-feed and Rosi-fast groups, ensuring similar synchrony between circadian and pharmacological interventions in both groups. PBS was injected in parallel with the feeding phase as the vehicle control (Veh). This dose is equal to 2.5 mg/kg daily dose for regular treatment, for which reason the adverse effect on inducing bone loss by the 5-wk treatment was not obvious. The eWAT and sWAT samples were collected at 3 days after the final Rosi administration, with mice returning to normal ad libitum feeding in the interim to minimize potential acute effects of drug administration or severe metabolic challenges. We conducted the RNA-seq for eWAT and sWAT from the vehicle control, Rosi-Fast, Rosi-Feed groups and investigated the expression changes of Rosiglitazone treatment. GSEA (v4.0) was used to perform the Gene Set Enrichment Analysis and examine the effects of Rosiglitazone treatment in the biological pathways.[38]

Transcription factor enrichment analysis

Transcription factor (TF) enrichment analysis was performed using ChEA3.[18] ChEA3 integrates the ChIP-Seq, co-expression, and co-occurrence (biological function) to determine the target genes of TFs. For the TF enrichment analysis of the genes with down-regulated GElaS during aging. We calculated the enrichment rank score for each TF by ChEA3[18] in the genes with down-regulated GElaS during aging in eWAT and sWAT, separately. The average of enrichment rank score between eWAT and sWAT was computed and the criteria of average score < 100 was adopted to identify the candidate TFs enriched in the genes with down-regulated GElaS during aging (Figure 4A).

Bone processing and bone marrow fat analysis

Femurs were collected and fixed in 10% neutral buffered formalin (Sigma) overnight at 4 °C, and subsequently used for bone micro-architecture analysis and bone marrow fat quantification. For micro-architecture analysis, a Quantum FX μCT Scanner (Perkin-Elmer) was used for scanning. For bone marrow fat quantification, femurs were decalcified in a 14% EDTA solution for at least 2 weeks with frequent change of solution. The bones were then stained for 48 hours in 1% osmium tetroxide, 2.5% potassium dichromate solution at RT, washed in tap water for at least 2 hours, and imaged by μCT. The software Analyze 12.0 was used to quantify lipid volume and μCT scan parameters according to the bone micro-architecture add-on. Marrow adipose sections were determined based on consistent 250 slice intervals measured from the identified growth plate of the femur.

Metabolic parameters in the chow-HFD-chow cycle during aging

Young (2 months) and aged (18 months) animals were undergone a chow-HFD-chow cycle, separately. The treatment for HFD and chow diet followed by HFD are both for one week. The metabolic parameters including body weight, fat mass, and lean mass were measured by mouse Magnetic resonance imaging (MRI) at start and end of HFD switch and at one week of chow diet after HFD treatment. Tail blood were collected at these time points to measure glucose, insulin, and free fat acid (according to the above description methods) in the chow-HFD-chow cycle for young and aged mice.

GElaS analysis during obesity

Mice at 8 weeks old were fed with HFD for 8 weeks and sacrificed at *ad libitum*, fasting, and refeeding states (as the above description). The epididymal adipose tissue (eWAT), inguinal adipose tissues (sWAT), liver, and gastrocnemius muscle were harvested from the animals in each state. We conducted the RNA sequencing for the metabolic organs in AL-F-R cycle during obesity. We mapped the RNA reads to the mouse reference genomes using the STAR (2.7.7a)[31] and calculated the read counts for each gene by featureCounts (v2.0.1).[32] The R package, limma (v3.44.3) was used to conduct the differentially expressed analysis.[34] GElaS was calculated as described above for the chow and HFD mice. We employed the same criteria to identify the differential elastic genes between chow and HFD mice. The functional enrichment analysis was performed as described above for the genes with down-regulated GElaS during obesity. The HFD snRNA-seq data was used to demonstrate the expression distribution for high (top 500) and low (bottom 500) GElaS genes from HFD mice.[8] The relationship between AgedvsYoung and HFDvsChow was conducted based on the Pearson's correlation.

QUANTIFICATION AND STATISTICAL ANALYSIS

The one-way ANOVA with Tukey's HSD post-hoc test was employed to calculate statistical significance for Figures 1A, 2A, 4D–4H, 4M, and 4N. The Mann-Whitney test was used to compute the p-value in Figures 1D, 2C, 3C, 4I, 5C, S1B, S2A, and S3F. The p-value of Figure S3G was computed by the Chi-squared Test. The p-values in Figures 3A, 3E, 3F, 5A, S3A, S4A, S4B, S4D, S4E, S4H, S4I, and S5A, were calculated by two-tailed Student's t-test. No specific statistical method was employed to determine whether the data exhibited a Gaussian distribution. p-value in Figure S1F was computed by Fisher's Exact test. A customary threshold of p-value < 0.05 was used to declare statistical significance. * and ** denote p-value < 0.05 and p-value < 0.01, respectively. Sample sizes are included in the figure legends.